RSC Advances

PAPER

View Article Online
View Journal | View Issue

Cite this: *RSC Adv.*, 2021, **11**, 38478

Defect induced electrocatalytic hydrogen properties of pentagonal PdX_2 (X = S, Se)†

Jingjing Li,[a] Dan Liang,[*a] Gang Liu,[*a] Baonan Jia,[a] Jingyu Cao,[a] Jinbo Hao[b] and Pengfei Lu[a]

Received 8th October 2021
Accepted 15th November 2021

DOI: 10.1039/d1ra07466k

rsc.li/rsc-advances

Searching for catalysts of hydrogen evolution reaction (HER) that can replace Pt is critical. Here, we investigated the HER electrocatalytic activity of pentagonal PdS_2 (penta-PdS_2) and $PdSe_2$ (penta-$PdSe_2$) by first-principles calculations. Three types of vacancies ($V_{S/Se}$, V_{Pd}, $DV_{S/Se}$) were constructed to activate the inert basal planes of PdS_2 and $PdSe_2$. The results show that S/Se and Pd vacancies significantly improve HER performance, and the Gibbs free energy (ΔG_H) of systems can be further regulated by vacancy concentration. Particularly, PdS_2 with 2.78% V_S, 50% V_{Pd} and $PdSe_2$ with 12.5% V_{Se} display the optimal ΔG_H value and the highest exchange current density. Further analysis of charge transfer and band structures were described that the introduce of vacancies efficiently regulates the electronic properties, resulting in the diminution of bandgap, and accelerates the charge transfer, thereby contributing to an enhanced electron environment for HER process. Our results provide a theoretical guidance for the applications of pentagonal transition-metal dichalcogenides as catalysts of hydrogen evolution reaction.

Introduction

Currently, pollution and the finite nature of fossil fuels make it extremely important to develop sustainable, recyclable and clean energy sources.[1–4] Hydrogen energy, prepared by hydrogen evolution reaction (HER), has attracted a lot of attention as an environmentally friendly and sustainable energy source.[5–14] Platinum (Pt), with minimal over-potential and slightly negative hydrogen adsorption free energy (ΔG_H), is considered to the best catalyst of HER.[15,16] However, the scarcity and high price of Pt limit its large-scale use. Therefore, it is urgent to develop abundant and inexpensive catalysts of HER that can replace Pt.[17–22]

Two-dimensional (2D) transition-metal dichalcogenides (TMDs) have attracted wide attention because of rich content, low price, high stability and high catalytic activity.[23–32] Many efforts have been made to use TMDs as alternative catalysts of Pt.[33–38] Recently, monolayer palladium diselenide ($PdSe_2$) crystals and palladium disulfide (PdS_2) with a novel puckered pentagonal structure have been demonstrated experimentally,[39–41] and PdS_2 has also shown more stable in pentagonal phase than in 1T phase.[42] Compared to the hexagonal structure, the puckered pentagonal structure shows some fascinating characteristics. The pentagonal structure exhibits anisotropy due to buckling breaking the symmetry of the lattice and enhances spin coupling.[43] Besides, it has a wide adjustable bandgap, ultra high air stability and high electron mobility.[44] Our previous work elucidated that the HER catalytic activity of 1T-MX_2 (M = Pt, Pd; X = S, Se, Te) with metal, non-metal atom doping and vacancies.[45] Lin *et al.* explored that pentagonal $PdSe_2$ nanosheets show good HER activity and its active sites are located on boundary atoms.[46] Liang *et al.* demonstrated that oxidized 2D $PdSe_2$ can effectively enhance electronic properties and electrocatalytic activity.[47] Even with some initial exploration, our knowledge of pentagonal PdX_2 (X = S, Se) is far from adequate, especially to enhance its HER activity by defect design. It's worth to reveal the HER catalytic activity of pentagonal structure to extend the potential replacement of Pt.

Herein, on the basis of first-principles calculations, we constructed penta-PdS_2, -$PdSe_2$ and introduced three types of vacancies in pristine systems to explore adsorption sites, electrocatalytic performance, vacancy concentration and the origin of improved HER activity. Three types of vacancies include S/Se vacancy ($V_{S/Se}$), Pd vacancy (V_{Pd}) and double S/Se vacancies ($DV_{S/Se}$). We found that the HER activity can be significantly improved by vacancies, and vacancy concentration efficiently regulates the electrocatalytic performance. The origin of HER activity enhancement was elucidated by electronic properties and charge transfer.

[a]State Key Laboratory of Information Photonics and Optical Communications, School of Electronic Engineering, Beijing University of Posts and Telecommunications, Beijing 100876, China. E-mail: liangdan@bupt.edu.cn; liu_g@126.com

[b]School of Science, Xi'an University of Architecture and Technology, Xi'an 710055, Shaanxi, China

† Electronic supplementary information (ESI) available: The band structures of PdS_2 and $PdSe_2$ with SOC and without SOC and under different vacancy concentrations. See DOI: 10.1039/d1ra07466k

Computational details

The computations were performed by using Vienna *ab initio* simulation package (VASP) based on density functional theory (DFT).[48] The generalized gradient approximation (GGA) of Perdew–Burke–Ernzerhof (PBE) function was adopted to exchange–correction functional energy. The energy cutoff for the plane wave basis was set as 450 eV, and a $4 \times 4 \times 1$ k-point mesh was sampled in Brillouin zones by a Monkhorst–Pack. To avoid the interactions between two layers, we set a 15 Å vacuum space in the z-direction,[49] and the effect of spin was also considered. All structures were relaxed until the forces on each atom were less than 0.01 eV $Å^{-1}$, and 10^{-5} eV was set to energy convergence criteria for electronic and ionic iterations. The van der Waals (vdW) interaction was considered by using optPBE function.[50] Considering that Pd is a rather heavy element, the spin–orbit coupling (SOC) effect was also taken into account in band structure computations. We built a 2×2 periodic supercell containing 8 Pd atoms and 16 Se atoms for pristine penta-PdS_2 and -$PdSe_2$ to investigate HER catalytic performance. Different vacancy concentrations were considered by removing one S/Se atom from 54 atoms (36 Se), 36 atoms (24 Se), 24 atoms (16 Se), 12 atoms (8 Se), 6 atoms (4 Se) supercells, corresponding to the vacancy concentrations of 2.8%, 4.2%, 6.3%, 12.5% and 25% for $V_{S/Se}$, respectively. For V_{Pd}, the vacancy concentrations of 5.6%, 8.3%, 12.5%, 25% and 50% were constructed by removing one Pd atom from 54 atoms (18 Pd), 36 atoms (24 Pd), 24 atoms (8 Pd), 12 atoms (4 Pd), 6 atoms (2 Pd) supercells, respectively.

The hydrogen adsorption energy (ΔE_H) is calculated by using the equation:

$$\Delta E_H = E_{host+H} - E_{host} - \frac{1}{2}E_{H_2} \quad (1)$$

where E_{host}, E_{host+H}, and E_{H_2} represent the total energies of system, system with adsorbed hydrogen atom, and H_2 gas molecule, respectively.

The Gibbs free energy (ΔG_H) is a good descriptor of HER electrocatalytic performance, which can be expressed as:

$$\Delta G_H = \Delta E_H + \Delta E_{ZPE} - T\Delta S \quad (2)$$

where ΔE_{ZPE} is the difference of zero-point energies (ZPEs) and ΔS is the difference of vibration entropy between adsorbed hydrogen and gas phase hydrogen. T is the temperature (T = 298.15 K). The entropy of adsorbed hydrogen is ignored because it is too small, so ΔS can be represented as $\Delta S = -\frac{1}{2}S^0_{H_2}$, where $S^0_{H_2}$ is the entropy of H_2 gas molecule.[51] Therefore, the ΔG_H can be simplified to $\Delta G_H = \Delta E_H + 0.164$ eV.

Results and discussion

The geometric structure of pentagonal PdX_2 (X = S, Se) consists of X–M–X three-atom-thick layers, in which M layer is sandwiched with two X layers, as shown in Fig. 1a. Each M atom binds four X atoms in pentagonal phase, and each unit cell contains two M atoms and four X atoms (highlighted by shaded area in Fig. 1a). The space group is $P2_1/c$ (no. 14), which exhibits a smaller symmetry compared to the common 2H- and 1T-phase. The lattice parameters that we computed are a = 5.46 Å, b = 5.56 Å for PdS_2, and a = 5.71 Å, b = 5.88 Å for $PdSe_2$, agreeing well with previous theoretical studies (a = 5.47 Å, b = 5.57 Å for PdS_2, a = 5.74 Å, b = 5.91 Å for $PdSe_2$),[52] and experimental values of penta-$PdSe_2$ (a = 5.75 Å, b = 5.87 Å).[39] The unique puckering structure allows for the existence of two different metal–nonmetal bonds inside the structure, they are the bond formed by M with X above pucker (M–X1) and the bond formed by M with X below pucker (M–X2), respectively. The bond lengths of M–X1 (d_{M-X1}) and M–X2 (d_{M-X2}) are 2.36 and 2.34 Å in PdS_2, 2.49 and 2.47 Å in $PdSe_2$. The difference of bond lengths between M–X1 and M–X2 contributes to the diversity of lattice constants (a, b) along the different orientations in the surface of pentagonal structure. We obtained the vertical puckered distance (h) of the puckering pentagon is 1.29 Å in PdS_2 and 1.53 Å in $PdSe_2$, experimentally measured vertical thickness of $PdSe_2$ is 1.6 Å.[39]

For HER on the catalyst under acidic conditions, the first step is the adsorption of H atom *via* $H^+ + e^-$ + catalyst → H* − catalyst (Volmer process), where H* denotes H adsorbed to the catalyst. The second step is the release of H_2 molecules, which can be described as H* − catalyst + H* − catalyst → H_2 + catalyst (Tafel process) or H* − catalyst + $H^+ + e^-$ → H_2 + catalyst (Heyrovsky process). The hydrogen evolution activity of the catalyst can be expressed by the Gibbs free energy (ΔG_H). An efficient catalyst means that it has the adsorption and desorption capacity of H and the ability to combine H is neither too strong nor too weak ($|\Delta G_H| \approx 0$). Before exploring the adsorption behavior of H, we firstly determined the most stable adsorption site of H, the calculated adsorption energies (ΔE_H) were summarized in Table 1. For pristine PdS_2 and $PdSe_2$, three possible adsorption sites were selected, as shown in Fig. 1b, of which site 1 shows the lowest adsorption energy. Considering hydrogen adsorbed at site 1, PdS_2 and $PdSe_2$ show ΔG_H values of 0.96 eV and 1.03 eV, respectively. The positive and large values of ΔG_H indicate that the intrinsic structure does not adsorb H well enough to be catalytically inert. To improve the HER performance, we introduced vacancies in basal plane of PdS_2 and $PdSe_2$. The presence of elemental vacancies in materials are generally inevitable. Based on optimized intrinsic structures of PdS_2 and $PdSe_2$, we constructed three types of vacancies: a S/Se atom was removed from the surface to form S/Se atom vacancy ($V_{S/Se}$, Fig. 1c); a Pd atom was removed from the surface to form Pd atom vacancy (V_{Pd}, Fig. 1d); two adjacent Se atoms were removed from the surface to form a double Se atom vacancy ($DV_{S/Se}$, Fig. 1e). Compared with the intrinsic structure, the defective structures display some deformation around the vacancy after optimization, while the deformation is very weak, and the basic structures still maintain.

Similarly, we considered the possible H adsorption sites near the vacancy in defective structures. For V_S in PdS_2 and V_{Se} in $PdSe_2$ (Fig. 1c), site 1 has the lowest adsorption energy (Table 1), and when H is placed at site 2 and 5, H will move to the position of site 1 after optimization. As for V_{Pd} in PdS_2, site 5 and 1 have

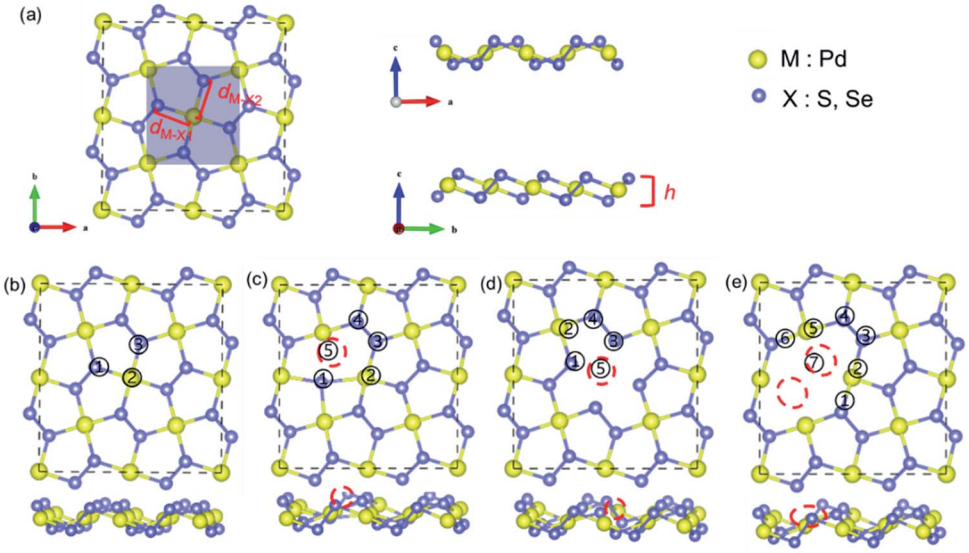

Fig. 1 Top and side views of (a) pentagonal PdX_2 (X = S, Se), (b) pristine PdX_2, (c) PdX_2 with S/Se-vacancy ($V_{S/Se}$), (d) PdX_2 with Pd-vacancy (V_{Pd}), (e) PdX_2 with double S/Se-vacancies ($DV_{S/Se}$). The yellow, purple balls represent Pd, S/Se, respectively. The red dashed circles are vacancy sites and the numbers denote adsorption positions of H considered in this work.

Table 1 Adsorption energy of H (ΔE_H/eV) at considered H-adsorption sites of PdS_2 and $PdSe_2$ marked in Fig. 1

Defect type	H-Adsorption sites	ΔE_H (eV) PdS_2	$PdSe_2$
Pristine	1	0.80	0.86
	2	1.51	1.35
	3	0.81	1.01
$V_{S/Se}$	1	−0.32	0.01
	2	—	—
	3	0.94	0.84
	4	0.62	0.97
	5	—	—
V_{Pd}	1	−0.43	−0.01
	2	−0.40	—
	3	0.70	−0.08
	4	0.01	0.46
	5	−0.52	0.72
DV_{Se}	1	0.20	0.50
	2	—	—
	3	0.47	0.55
	4	0.37	0.97
	5	—	—
	6	—	—
	7	−0.54	−0.54

the similar and low adsorption energy, and when the initial position of H is site 5, the bond length of the H with Se atom at site 1 is 2.7 Å and with Se atom at site 3 is 3.2 Å after structural relaxation, so we consider site 1 as the most stable H adsorption location for V_{Pd} in PdS_2. In $PdSe_2$ with V_{Pd}, the lowest energy positions are site 3 and site 1, when H is adsorbed at site 3, the H atom will shift to site 1 after structural relaxation, and the bond length formed with the Se atom at site 1 is 2.8 Å, coupled with the fact that the H adsorbed at site 2 will transfer to site 1, which indicates that the site 1 is the most stable adsorption site. For DV_S and DV_{Se}, the stable H adsorption sites are only site 1, 3, 4, 7, and site 7 displays the lowest adsorption energy. Summarily, site 1 is the most stable H adsorption site for single-vacancy, site 7 is the most stable H adsorption site for the double-vacancies. Hence, the following discussion is based on site 1 for $V_{S/Se}$ and V_{Pd} and site 7 for $DV_{S/Se}$.

It is obvious that three types of vacancies bring about a drastic decreasing effect in ΔG_H, as shown in Fig. 2. We constructed the same vacancy concentration in two systems. For PdS_2, the ΔG_H of 6.3% V_S reduces to −0.16 eV, which indicates an efficient regulation of hydrogen absorption. 12.5% V_{Pd} and DV_S vacancies more intensely modulate the ΔG_H, showing more negative ΔG_H values of −0.27 and −0.38 eV, respectively (Fig. 2a). For $PdSe_2$, 6.3% V_{Se} and 12.5% V_{Pd} have similar ΔG_H values of 0.16 and 0.15 eV (Fig. 2b), DV_{Se} has a largely negative ΔG_H value of −0.37 eV and shows the strongest influence on ΔG_H. It is noticed that double vacancies give rise to largely negative ΔG_H value both in PdS_2 and $PdSe_2$. The $|\Delta G_H|$ value of $PdSe_2$ with metallic vacancy (V_{Pd}) is much closer to zero than that of PdS_2, displaying a superior HER activity. Considering the approximate $|\Delta G_H|$ value of systems with V_S or V_{Se}, we observe that non-metallic vacancies result in a similar influence on PdS_2 and $PdSe_2$.

We took $V_{S/Se}$ and V_{Pd} vacancies to explore the influence of vacancy concentration on ΔG_H, 2.8%, 4.2%, 6.3%, 12.5% and 25% vacancy concentrations were constructed for $V_{S/Se}$, accordingly, 5.6%, 8.3%, 12.5%, 25% and 50% vacancy concentrations for V_{Pd}. Considering that the change in supercell size has an effect on the position of the double vacancies, coupled with the existence of interaction between two vacancies, we cannot be sure that it's an isolated effect of the vacancy concentration for the change of ΔG_H, so only the single vacancy

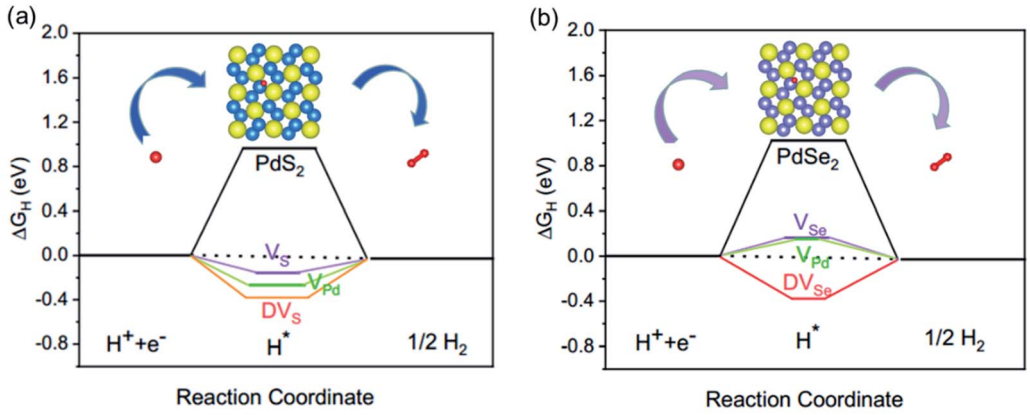

Fig. 2 HER free energy diagrams of pristine and defective (a) PdS_2 and (b) $PdSe_2$. The illustration represents the adsorption process of H.

with different concentrations was adopted in this study. The curves of ΔG_H value with different vacancy concentrations were plotted in Fig. 3. The results show that with the increase of $V_{S/Se}$ concentration, ΔG_H values display a decrease tendency (Fig. 3a). $PdSe_2$ with V_{Se} exhibits better HER performance than PdS_2 with V_S. The ΔG_H value is more sensitive to low $V_{S/Se}$ concentration, and in the case of high concentration, $V_{S/Se}$ concentration has little effect on the ΔG_H. It is also seen that the ΔG_H values decrease first and then increase with increasing V_{Pd} concentration both in PdS_2 and $PdSe_2$ (Fig. 3b). $PdSe_2$ shows good HER activity with V_{Pd} concentration in the range between 5.6% and 25%, and PdS_2 reaches the optimal ΔG_H value (−0.04 eV) at 50% V_{Pd} concentration.

In order to intuitively represent the hydrogen evolution activity of the defective structure with different vacancy concentrations, we calculated the exchange current density (i_0), which characterized the transfer efficiency of protons from solution to catalyst surface. Under standard conditions (pH = 0 and $T = 300$ K), if $\Delta G_H < 0$, i_0 can be calculated by the following formula:

$$i_0 = -ek_0 \frac{1}{1 + \exp(-\Delta G_H/kT)} \quad (3)$$

Inversely, if $\Delta G_H > 0$, i_0 is represented as

$$i_0 = -ek_0 \frac{1}{1 + \exp(-\Delta G_H/kT)} \exp(-\Delta G_H/kT) \quad (4)$$

where k is the Boltzmann constant and k_0 is the rate constant (k_0 = 200 per s per site). For pristine PdS_2 and $PdSe_2$, the ΔG_H values of 0.96 and 1.03 eV have log i_0 of −33 and −34 A per site, respectively. The other calculated results were represented by volcano curve plotted in Fig. 4a. Among them, PdS_2 with 2.78% V_S, 50% V_{Pd} and $PdSe_2$ with 12.5% V_{Se} are located at the top of the volcano curve, indicating the optimal ΔG_H value and the highest exchange current density (~10^{-18} A per site). In particular, PdS_2 requires only a small concentration of S vacancy to achieve excellent hydrogen evolution activity. The change of vacancy concentration will lead to the variation of electron environment, and it is important to reveal the inherent charge transfer properties. We calculated the Bader charge of adsorbed H in different vacancy concentrations. As shown in Fig. 4b, there are two cases of charge transfer: when H is adsorbed on PdS_2, the electrons are transferred from H to PdS_2 in most cases; and when H is adsorbed on $PdSe_2$, the adsorbed H gets electrons from $PdSe_2$. This is because the electronegativity of the atoms connected to H is different, and the electronegativity of S

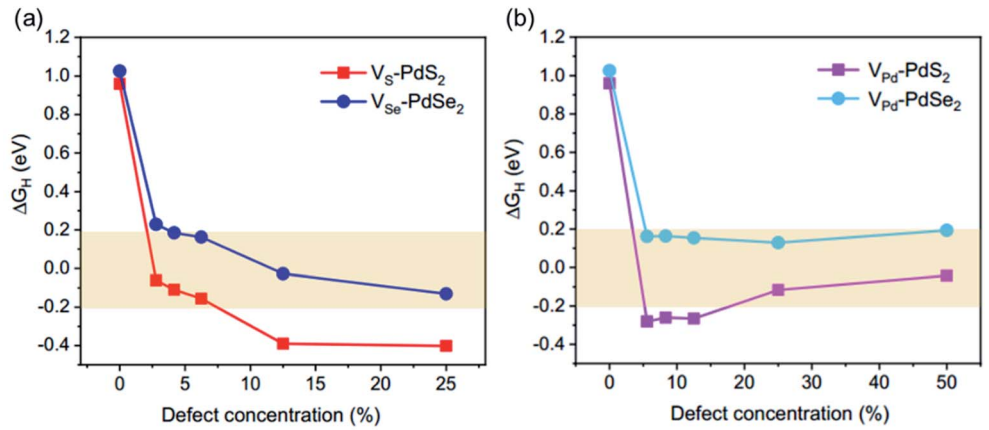

Fig. 3 ΔG_H values of defective (a) PdS_2 and (b) $PdSe_2$ as a function of vacancy concentration.

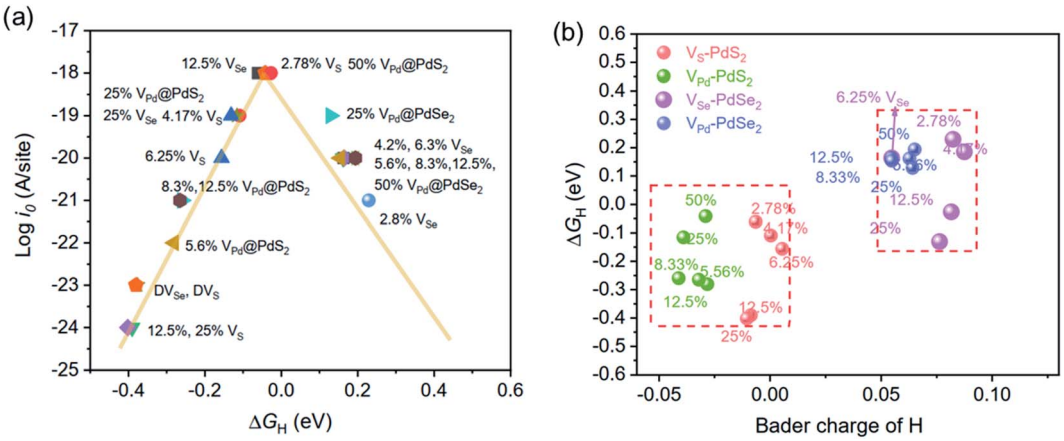

Fig. 4 (a) The exchange current density i_0 as a function of ΔG_H values. (b) The relationship of ΔG_H with Bader charges of adsorbed H in PdS/Se_2 with different vacancy concentrations.

is larger than that of Se, which has an effect on the Bader charge of adsorbed H and thus affects the value of ΔG_H. This is also consistent with our previous study.[45]

Based on previous investigations, we know that the vacancies give rise to the variation in electronic properties, consequently the improved catalytic performance. As shown in Fig. 5a, the total density of states (TDOS) of defective $PdSe_2$ shows that a large gap state is generated near the Fermi level compared to pristine system, resulting in the bandgap reduction. These new states are attributed to the states resulting from vacancies that are introduced into pristine system. The gap states are beneficial to electron transfer and the conductivity of defective structures and this change may convert the system from being semiconductor to exhibiting metallic properties. We analysed the projected density of states (PDOS) of three defective $PdSe_2$ structures in Fig. 5b–d. It is found that the gap states near the Fermi level are mainly contributed by 4d orbital of Pd and 3p orbital of Se near vacancies. From TDOS and PDOS, it demonstrates that the vacancies effectively modify the electronic structure and increase the occupied states of d and p electrons

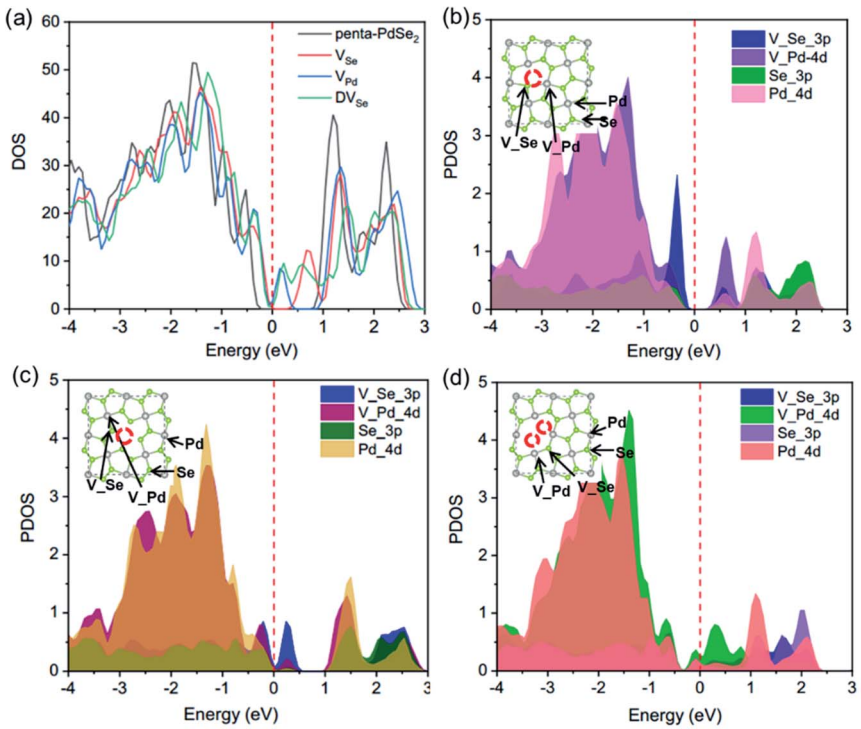

Fig. 5 (a) Total density of states (TDOS) of pristine $PdSe_2$ and three defective structures. Projected density of states (PDOS) of Pd 4d and Se 3p orbitals in $PdSe_2$ with (b) V_{Se}, (c) V_{Pd} and (d) DV_{Se}. The insets denote the positions of special Se, Pd. For V_{Se} indicates the Se atom closest to vacancy.

near the Fermi level, thus affecting the adsorption of H and improving the hydrogen evolution activity.

To further explore charge transfer mechanism between defective structures and H, the differential charge transfer density ($\Delta\rho(r)$) of pristine $PdSe_2$ and three defective structures were calculated. The $\Delta\rho(r)$ is calculated as

$$\Delta\rho(r) = \rho_{cat+H}(r) - \rho_{cat}(r) - \rho_{H}(r) \quad (5)$$

where $\rho_{cat+H}(r)$, $\rho_{cat}(r)$, and $\rho_{H}(r)$ denote charge density of catalyst with adsorbed H, without H and H atom, respectively. The calculated $\Delta\rho(r)$ results were plotted in Fig. 6. On pristine systems without adsorbed H, Se has a negative charge and Pd has a positive charge. After the adsorption of H atom, p electrons with a negative $\Delta\rho(r)$ appear around Pd atom (Fig. 6a), which indicates that the adsorption of H leads to a slight backward charge transfer of systems. Meanwhile, for $PdSe_2$, the adsorption of H causes electrons to transfer from the substrate to H, and the introduction of vacancies arouses more electrons to transfer and a redistribution. That is to say, the introduction of vacancies promotes rapid charge transfer, which is responsible for the improvement of HER activity.

The band structures of PdS_2 and $PdSe_2$ at different vacancy concentrations were calculated to explore the effect of vacancy concentration on electronic properties. As the SOC has a significant impact on the electronic properties, especially for heavy atoms, we firstly considered the influence of SOC on the band structures of PdS_2 and $PdSe_2$, taking 12.5% V_S and V_{Se} as an example. Comparing the bands obtained with and without SOC (Fig. S1†), there are splitting bands in the band structures due to the spin–orbit coupling, and the SOC effect slightly alters the bandgap value, a bandgap difference of 0.02–0.03 eV obtained in two cases. While we believe that the SOC effect in PdS_2 and $PdSe_2$ is not obvious and especially will not affect the variation trend of electronic structure resulting from the introduction of vacancies, thereby in the subsequent band structure calculations, the SOC is not included.

From the calculated results of band structures (Fig. S2†) and the bandgap values (Table 2) of PdS_2 and $PdSe_2$ with different vacancy concentrations, it is found that with the increase of vacancy concentration, the band states would approach to the Fermi level and the position of the valence band maximum (VBM) and the conduction band minimum (CBM) would also change accordingly, thus resulting in the decrease of the bandgap, which leads to the enhancement of the adsorption capacity of H near the vacancy site.

Table 2 The minimum bandgap values (eV) of $V_{S/Se}$, V_{Pd} in PdS_2 and $PdSe_2$ with different vacancy concentrations

$V_{S/Se}$	PdS_2	$PdSe_2$	V_{Pd}	PdS_2	$PdSe_2$
0	1.21	1.43	0	1.21	1.43
2.8%	0.83	0.86	5.6%	0.11	0.40
4.2%	0.71	0.74	8.3%	—	0.31
6.3%	0.69	0.67	12.5%	—	0.31
12.5%	0.39	0.43	25%	—	—
25%	—	—	50%	—	—

For PdS_2, the intrinsic structure has an indirect bandgap of 1.21 eV, which is consistent with previous studies,[53] and after the introduction of S vacancy, the bandgap gradually decreases with the increase of the vacancy concentration, and exhibits metallicity when the V_S concentration reaches to 25%. In comparison, PdS_2 with V_{Pd} displays a smaller bandgap and shows metallic properties as soon as the concentration increases to 8.3%. The intrinsic $PdSe_2$ has an indirect bandgap of 1.43 eV, agreeing well with the experimental value.[39] Similarly, the bandgap of $PdSe_2$ with V_{Se} decreases with vacancy concentration and appears metallicity at 25% V_{Se} concentration. For $PdSe_2$ with V_{Pd}, it shows metallicity only when the vacancy concentration increases to 25%. It's found that PdS_2 with V_{Pd} reveals the stronger metallic than $PdSe_2$ under the same V_{Pd} concentration, which is also consistent with our calculated HER performance. We noticed that the hydrogen adsorption capacity gradually increases when the bandgap is decreasing, and when the defect concentration reaches a certain value, the bandgap no longer changes and the hydrogen adsorption capacity then changes very little, which is also consistent with our calculated HER activity (Fig. 3). The HER adsorption capacity of V_S increases continuously with the defect concentration, while the H adsorption capacity of V_{Pd} does not continue to enhance when reaching 5.6% PdS_2 and 12.5% $PdSe_2$ and shows a slightly increasing trend. The existence of vacancy efficiently regulates the electronic properties, resulting in the diminution of bandgap, and accelerates the charge transfer,

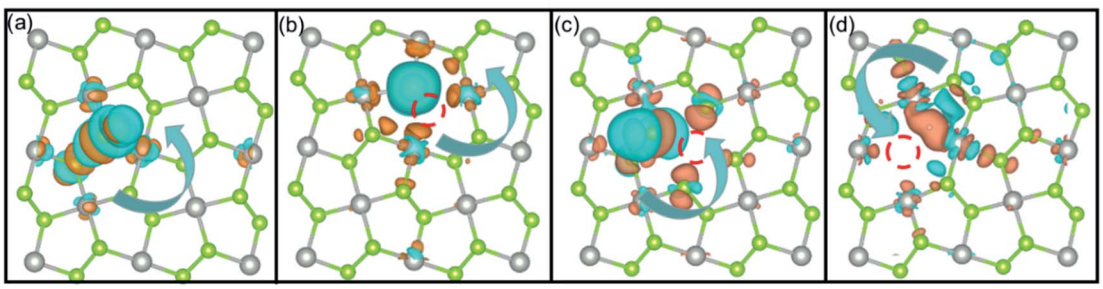

Fig. 6 Differential charge density of (a) pristine $PdSe_2$ and $PdSe_2$ with (b) V_{Se}, (c) V_{Pd}, (d) DV_{Se}. The orange regions represent charge accumulation and the blue regions stand for electron depletion. The red dashed circles indicate the positions of vacancies.

thereby contributing to an enhanced electron environment for HER process.

Conclusions

We explored the HER activity of penta-PdS_2 and -$PdSe_2$ by first-principles calculations. The most stable adsorption site of H was determined by comparing the adsorption energy of possible sites. Our results show that the S/Se and Pd vacancies can significantly improve HER performance of PdS_2 and $PdSe_2$, and the origin of improvement in HER activity was elucidated through density of states and charge transfer. Moreover, the influence of vacancy concentration on the HER performance was investigated. The ΔG_H values display a decrease tendency with the increase of $V_{S/Se}$ concentration, and $PdSe_2$ with V_{Se} exhibits better HER performance than PdS_2 with V_S. It is also found that the ΔG_H values decrease first and then increase with increasing V_{Pd} concentration both in PdS_2 and $PdSe_2$. PdS_2 with 2.78% V_S, 50% V_{Pd} and $PdSe_2$ with 12.5% V_{Se} are located at the top of the volcano curve, indicating the optimal ΔG_H value and the highest exchange current density. Further analysis of Bader charge and band structures were described that the increase of vacancy concentration reduces the bandgap and affects the electron environment. Our results provide a theoretical guidance for electrocatalytic applications of pentagonal transition-metal dichalcogenides.

Conflicts of interest

There are no conflicts to declare.

Acknowledgements

This work was supported by the Open-Foundation of Key Laboratory of Laser Device Technology, China North Industries Group Corporation Limited (No. KLLDT202001), and Fund of State Key Laboratory of IPOC (BUPT), P. R. China (No. IPOC2019ZZ04). We thank for the helpful discussion with Prof. Pengfei Guan and the computational support from the Beijing Computational Science Research Center (CSRC).

Notes and references

1 N. S. Lewis and D. G. Nocera, *Proc. Natl. Acad. Sci. U. S. A.*, 2006, **103**, 15729–15735.
2 X. He, S. Luan, L. Wang, R. Wang, P. Du, Y. Xu, H. Yang, Y. Wang, K. Huang and M. Lei, *Mater. Lett.*, 2019, **244**, 78–82.
3 B. Hinnemann, P. G. Moses, J. Bonde, K. P. Jørgensen, J. H. Nielsen, S. Horch, I. Chorkendorff and J. K. Nørskov, *J. Am. Chem. Soc.*, 2005, **127**, 5308–5309.
4 M. G. Walter, E. L. Warren, J. R. McKone, S. W. Boettcher, Q. Mi, E. A. Santori and N. S. Lewis, *Chem. Rev.*, 2010, **110**, 6446–6473.
5 X. Geng, W. Sun, W. Wu, B. Chen, A. Al-Hilo, M. Benamara, H. Zhu, F. Watanabe, J. Cui and T.-p. Chen, *Nat. Commun.*, 2016, **7**, 1–7.
6 S. Lin, J. C. Liu, W. Z. Li, D. Wang, Y. Huang, C. Jia, Z. W. Li, M. Murtaza, H. Y. Wang, J. N. Song, Z. L. Liu, K. Huang, D. Zu, M. Lei, B. Hong and H. Wu, *Nano Lett.*, 2019, **19**, 6853–6861.
7 W. J. Zou, K. P. Dou, Q. Jiang, J. D. Xiang, C. C. Kaun and H. Tang, *RSC Adv.*, 2019, **9**, 39951–39957.
8 D. Senthilnathan, P. Giunta, V. Vetere, A. Kachmar, P. Maldivi and A. A. Franco, *RSC Adv.*, 2014, **4**, 5177–5187.
9 L. B. Yang, P. Gao, J. H. Lu, W. Guo, Z. Zhuang, Q. Q. Wang, W. J. Li and Z. Y. Feng, *RSC Adv.*, 2020, **10**, 20654–20664.
10 S. C. Chan, Y. L. Cheng, B. K. Chang and C. W. Hong, *RSC Adv.*, 2021, **11**, 18500–18508.
11 M. C. He, F. P. Kong, G. P. Yin, Z. Lv, X. D. Sun, H. Y. Shi and B. Gao, *RSC Adv.*, 2018, **8**, 14369–14376.
12 H. Ogihara, M. Fujii and T. Saji, *RSC Adv.*, 2014, **4**, 58660–58663.
13 Z. Y. Guo, Q. X. Ma, Z. W. Xuan, F. L. Du and Y. Zhong, *RSC Adv.*, 2016, **6**, 16730–16735.
14 L. Wu, X. H. Guo, Y. Xu, Y. F. Xiao, J. W. Qian, Y. F. Xu, Z. Guan, Y. H. He and Y. Zeng, *RSC Adv.*, 2017, **7**, 32264–32274.
15 J. Greeley, I. Stephens, A. Bondarenko, T. Johansson, H. Hansen, T. Jaramillo and J. Rossmeisl, *Nat. Chem.*, 2009, **1**, 7.
16 J. Greeley, T. F. Jaramillo, J. Bonde, I. Chorkendorff and J. K. Nørskov, *Nat. Mater.*, 2006, **5**, 909–913.
17 P. Du and R. Eisenberg, *Energy Environ. Sci.*, 2012, **5**, 6012–6021.
18 E. J. Popczun, J. R. McKone, C. G. Read, A. J. Biacchi, A. M. Wiltrout, N. S. Lewis and R. E. Schaak, *J. Am. Chem. Soc.*, 2013, **135**, 9267–9270.
19 Q. Liu, J. Tian, W. Cui, P. Jiang, N. Cheng, A. M. Asiri and X. Sun, *Angew. Chem., Int. Ed.*, 2014, **53**, 6710–6714.
20 W. Zhong, B. Xiao, Z. Lin, Z. Wang, L. Huang, S. Shen, Q. Zhang and L. Gu, *Adv. Mater.*, 2021, **33**, 2007894.
21 S. Ma, J. Deng, Y. Xu, W. Tao, X. Wang, Z. Lin, Q. Zhang, L. Gu and W. Zhong, *J. Energy Chem.*, 2022, **66**, 560–565.
22 D. Wang, D. Zhang, C. Tang, P. Zhou, Z. Wu and B. Fang, *Catal. Sci. Technol.*, 2016, **6**, 1952–1956.
23 J. D. Benck, T. R. Hellstern, J. Kibsgaard, P. Chakthranont and T. F. Jaramillo, *ACS Catal.*, 2014, **4**, 3957–3971.
24 A. B. Laursen, S. Kegnæs, S. Dahl and I. Chorkendorff, *Energy Environ. Sci.*, 2012, **5**, 5577–5591.
25 D. Merki and X. Hu, *Energy Environ. Sci.*, 2011, **4**, 3878–3888.
26 P. C. Vesborg, B. Seger and I. Chorkendorff, *J. Phys. Chem. Lett.*, 2015, **6**, 951–957.
27 Q. M. Wang, J. M. Zhang, Z. D. Zhang, Y. N. Hao and K. Bi, *Adv. Compos. Hybrid Mater.*, 2020, **3**, 58–65.
28 J. C. Xu, J. Q. Cao, M. H. Guo, S. L. Yang, H. M. Yao, M. Lei, Y. N. Hao and K. Bi, *Adv. Compos. Hybrid Mater.*, 2021, **4**, 761–767.
29 P. Lu, *J. Sichuan Norm. Univ., Nat. Sci.*, 2020, **043**, 1–20.
30 J. Mou, Y. Gao, J. Wang, J. Ma and H. Ren, *RSC Adv.*, 2019, **9**, 11755–11761.
31 J. M. Ge, J. X. Jin, Y. M. Cao, M. H. Jiang, F. Z. Zhang, H. L. Guo and X. D. Lei, *RSC Adv.*, 2021, **11**, 19630–19638.

32 L. Song, M. J. Zhao, X. X. Li, Z. P. Zhang and L. T. Qu, *RSC Adv.*, 2016, **6**, 70740–70746.
33 M. Chhetri, U. Gupta, L. Yadgarov, R. Rosentsveig, R. Tenne and C. Rao, *Dalton Trans.*, 2015, **44**, 16399–16404.
34 D. Liang, Y.-W. Zhang, P. Lu and Z. G. Yu, *Nanoscale*, 2019, **11**, 18329–18337.
35 C. Tsai, F. Abild-Pedersen and J. K. Nørskov, *Nano Lett.*, 2014, **14**, 1381–1387.
36 Y. Xu, L. Wang, X. Liu, S. Zhang, C. Liu, D. Yan, Y. Zeng, Y. Pei, Y. Liu and S. Luo, *J. Mater. Chem. A*, 2016, **4**, 16524–16530.
37 X. N. Guan, R. Zhang, B. N. Jia, L. Y. Wu, B. Zhou, L. Fan, G. Liu, Y. Wang, P. F. Lu and G. D. Peng, *J. Non-Cryst. Solids*, 2020, **550**, 7.
38 Z. Wang, B. Xiao, Z. Lin, Y. Xu, Y. Lin, F. Meng, Q. Zhang, L. Gu, B. Fang, S. Guo and W. Zhong, *Angew. Chem.*, 2021, **60**, 23388–23393.
39 A. D. Oyedele, S. Yang, L. Liang, A. A. Puretzky, K. Wang, J. Zhang, P. Yu, P. R. Pudasaini, A. W. Ghosh, Z. Liu, C. M. Rouleau, B. G. Sumpter, M. F. Chisholm, W. Zhou, P. D. Rack, D. B. Geohegan and K. Xiao, *J. Am. Chem. Soc.*, 2017, **139**, 14090–14097.
40 A. Guha, R. Sharma, K. R. Sahoo, A. B. Puthirath, N. Shyaga, P. M. Ajayan and T. N. Narayanan, *ACS Appl. Energy Mater.*, 2021, **4**, 8715–8720.
41 S. Jiang, C. Zhang, E. Zhao, M. Han, L. Zhu and Y.-Q. Zhao, *Appl. Surf. Sci.*, 2021, **570**, 151178.
42 D. Saraf, S. Chakraborty, A. Kshirsagar and R. Ahuja, *Nano Energy*, 2018, **49**, 283–289.
43 R. Quhe, R. Fei, Q. Liu, J. Zheng, H. Li, C. Xu, Z. Ni, Y. Wang, D. Yu, Z. Gao and J. Lu, *Sci. Rep.*, 2012, **2**, 1–6.
44 M. Long, Y. Wang, P. Wang, X. Zhou, H. Xia, C. Luo, S. Huang, G. Zhang, H. Yan, Z. Fan, X. Wu, X. Chen, W. Lu and W. Hu, *ACS Nano*, 2019, **13**, 2511–2519.
45 G. Liu, J. Li, C. Dong, L. Wu, D. Liang, H. Cao and P. Lu, *Int. J. Hydrogen Energy*, 2021, **46**, 18294–18304.
46 Z. Lin, B. Xiao, Z. Wang, W. Tao, S. Shen, L. Huang, J. Zhang, F. Meng, Q. Zhang, L. Gu and W. Zhong, *Adv. Funct. Mater.*, 2021, **31**, 2102321.
47 Q. Liang, Q. Zhang, J. Gou, T. Song, Arramel, H. Chen, M. Yang, S. X. Lim, Q. Wang, R. Zhu, N. Yakolev, S. C. Tan, W. Zhang, K. S. Novoselov and A. T. Wee, *ACS Nano*, 2020, **14**, 5668–5677.
48 K. Momma and F. Izumi, *J. Appl. Crystallogr.*, 2011, **44**, 1272–1276.
49 L. Seixas, A. Carvalho and A. C. Neto, *Phys. Rev. B: Condens. Matter Mater. Phys.*, 2015, **91**, 155138.
50 S. Grimme, *J. Comput. Chem.*, 2004, **25**, 1463–1473.
51 J. K. Nørskov, T. Bligaard, A. Logadottir, J. Kitchin, J. G. Chen, S. Pandelov and U. Stimming, *J. Electrochem. Soc.*, 2005, **152**, J23.
52 W. Xiong, K. Huang and S. Yuan, *J. Mater. Chem. C*, 2019, **7**, 13518–13525.
53 H. Yang, Y. Li, Z. Yang, X. Shi, Z. Lin, R. Guo, L. Xu, H. Qu and S. Zhang, *Vacuum*, 2020, **174**, 109176.